Ischemic Stroke Reduces Bone Perfusion and Alters Osteovascular Structure

Nicholas J. Hanne, PhD[a], Andrew J. Steward, PhD[a], Carla Geeroms[b], Elizabeth D. Easter[c], Hannah L. Thornburg[a], Greet Kerckhofs, PhD[b,d,e], Tatjana Parac-Vogt, PhD[f], Huaxin Sheng, MD[g], Jacqueline H. Cole, PhD*[,a]

[a] Joint Department of Biomedical Engineering, University of North Carolina, Chapel Hill, NC, and North Carolina State University, Raleigh, NC, USA

[b] Prometheus, Division of Skeletal Tissue Engineering, KU Leuven, Leuven, Belgium

[c] Materials Science and Engineering, North Carolina State University, Raleigh, NC, USA

[d] Institute of Mechanics, Materials and Civil Engineering, UC Louvain, Louvain-la-Neuve, Belgium

[e] Materials Engineering, KU Leuven, Leuven, Belgium

[f] Department of Chemistry, KU Leuven, Leuven, Belgium

[g] Department of Anesthesiology, Duke University Medical Center, Durham NC, USA

Short title: Stroke Alters Osteovascular Structure and Function

***Corresponding Author:**
Jacqueline H. Cole
Joint Department of Biomedical Engineering
University of North Carolina and North Carolina State University
911 Oval Drive
Campus Box 7115
Raleigh, NC 27695-7115
Tel: 919-515-5955
Fax: 919-513-3814
jacquecole@ncsu.edu

Abstract

Rationale: Stroke patients lose bone mass and experience fracture at an elevated rate. Although functional intraosseous vasculature is necessary for skeletal maintenance, the effect of stroke on osteovasculature is unknown. Objective: To characterize changes to osteovascular function, structure, and composition following mild-to-moderate-severity ischemic stroke in mice, both with and without exercise therapy. Methods and Results: Twelve-week-old male mice (n=27) received either a stroke (middle cerebral artery occlusion) or sham procedure, followed by four weeks of daily treadmill or sedentary activity. Intraosseous perfusion, measured weekly in the proximal tibial metaphysis, was reduced by stroke for two weeks. In the second week of recovery, exercise nearly restored perfusion to sham levels, and perfusion tended to be lower in the stroke-affected limb. At the conclusion of the study, osteovascular structure was assessed with contrast-enhanced computed tomography in the distal femoral metaphysis. Stroke significantly increased osteovascular volume and branching but reduced the relative number of blood vessels close to bone surfaces (6-22 μm away) and increased the relative number more than 52 μm away. These differences in vessel proximity to bone were driven by changes in the stroke-exercise group, indicating compounded effects of stroke and exercise. Exercise, but not stroke, nearly reduced the amount of osteogenic Type H blood vessels in the proximal tibial metaphysis, quantified with immunofluorescence microscopy. Conclusions: This study is the first to examine the effects of stroke on osteovasculature. Stroke increased the amount of osteovasculature, but since blood vessels close to bone are associated with bone remodeling, the shift in osteovascular structure could play a role in bone loss following stroke. The exercise-induced reduction in the amount of Type H vessels and the stroke-exercise effect on osteovascular structure suggest moderate aerobic activity may have detrimental effects on bone remodeling during early stroke recovery.

Keywords

ischemic stroke, bone vasculature, intraosseous perfusion

Non-standard Abbreviations and Acronyms

Ad.D – Adipocyte density

Ad.Th – Adipocyte thickness

Ad.V/Ma.V – Adipocyte volume per marrow volume

EMCN - Endomucin

LDF – Laser Doppler flowmetry

Ves.D – Blood vessel density

Ves.Th – Blood vessel thickness

Ves.S-BS – Vessel surface to bone surface distance

Ves.V/Ma.V – Vessel volume per marrow volume

Introduction

Stroke is the leading cause of disability in the US, as well as one of the leading causes worldwide [1]. Stroke not only causes cognitive and motor impairments but also negatively affects skeletal health [2–8]. Stroke patients lose bone mass at an accelerated rate, fall more, and experience hip fracture 2-4 times more frequently than individuals of the same age who have not experienced stroke [2,3,5]. Because bone adapts to altered mechanical loading [9], and bone mineral density (BMD) loss and fracture preferentially affect the paretic limbs [6,7], hemiplegia and limb disuse are thought to be solely responsible for these skeletal deficits post-stroke [4,6,8]. In addition, rehabilitation activity and exercise are correlated with reduced fracture risk and improved skeletal health outcomes following stroke [3,10–13], further supporting loading as a primary driver. However, a study in severe stroke patients showed lower BMD in various sites on the stroke-affected side, relative to the unaffected side, despite complete bedrest [8]. Even after controlling for activity level and other factors, lower vascular elasticity, a metric of vascular health, has been associated with lower polar stress-strain index, a surrogate measure of bone torsional stiffness and strength [14], in the radial diaphysis [15]. Together these results suggest that the negative effects of stroke on bone extend beyond just mechanical unloading and that vascular deficits may also contribute.

Because vasculature is critically important for maintaining functional bone tissue, supplying not only oxygen and nutrients but also cell signaling factors [16], vascular dysfunction may contribute to the increased fracture risk experienced by stroke patients. Little is known about the effects of stroke on limb vasculature, in particular on vascular perfusion and structure, and no previous study has examined the effects on the vasculature within bone, or *osteovasculature*. Two previous studies reported decreased blood flow in the affected lower leg compared to the

60 unaffected leg in elderly chronic stroke patients with mild-to-moderate gait asymmetry at least 6
61 months after moderate ischemic stroke [17,18]. Changes to limb blood flow, however, may not be
62 indicative of changes to osteovasculature, which has more direct impacts on bone remodeling and
63 the marrow microenvironment. In osteoporotic individuals, increased intraosseous perfusion
64 measured by contrast-enhanced clinical imaging was strongly correlated with increased bone
65 formation rate in the iliac crest [19] and weakly correlated with higher BMD in the proximal femur
66 [20]. In addition, an increased number of capillaries have been observed within 50 μm of bone
67 surfaces at active remodeling sites, compared to non-remodeling bone surfaces, in both humans
68 [21] and rats [22]. Within long bones, endothelial cells that express both endomucin (EMCN) and
69 CD31 (*Type H cells*) have been shown to regulate osteogenesis in mice [23,24]. The effects of
70 stroke on these osteovascular metrics (perfusion, structure, and cellular composition) are unknown
71 and may provide insight into the relationship between bone vasculature and bone loss following
72 stroke. Although characterizing osteovasculature in humans is difficult, it can be examined in
73 animal models, such as the established rodent models of ischemic stroke involving middle cerebral
74 artery occlusion (MCAo) [25,26].

75 In our previous study using an MCAo mouse model, we showed that although stroke did
76 not cause detrimental changes to bone microstructure, it prevented the exercise-induced
77 microstructural gains observed in the sham group, even without changes to limb coordination
78 during gait [27]. Since bone and vascular health are tightly coupled, we hypothesized that stroke
79 negatively impacts osteovasculature and inhibits the positive effects of treadmill exercise. In this
80 study, we used the same bones to characterize changes to *in vivo* functional intraosseous perfusion,
81 blood vessel network microstructure, and endothelial cellular composition following ischemic
82 stroke.

Methods

Study Design

All procedures were approved by North Carolina State University's Animal Care and Use Committee. Animals were group housed 4-5 per cage with a 12-hour diurnal light cycle and free access to standard chow and water. Twenty-seven male C57Bl/6J mice (The Jackson Laboratory, Bar Harbor, ME) received either an ischemic stroke (n = 15) or sham surgery (n = 12) at twelve weeks of age (Fig. 1). Mice were housed individually with wetted food and hydrogel packs for four days following surgery during the acute recovery period. After this period, they were returned to their original group cages and split into either daily treadmill exercise groups (n = 6 sham-exercise, n = 8 stroke-exercise) or sedentary control groups (n = 6 sham-sedentary, n = 7 stroke-sedentary). Surgery and exercise groups were randomly assigned to cages. Body mass was measured twice a day for the four days following surgery and weekly thereafter. Stroke recovery and sensorimotor function were assessed daily for four days following stroke and weekly thereafter. Intraosseous perfusion was measured with laser Doppler flowmetry (LDF) during the stroke or sham surgery and then weekly thereafter. After four weeks of stroke recovery with treadmill or sedentary activity, the mice were euthanized with CO_2 asphyxiation followed by cervical dislocation. Femora and tibiae from both left (stroke-affected) and right (stroke-unaffected) hindlimbs were collected. A subset of both affected and unaffected femora from six mice (n = 1 sham-sedentary, n = 2 sham-exercise, n = 1 stroke-sedentary, n = 2 stroke-exercise) were fixed for 16 hours in 5% neutral buffered formalin at 4°C and then stored in 1X phosphate buffered saline (PBS) at 4°C until assessment of osteovascular structure. All other bones were fixed for 18 hours in 10% neutral buffered formalin at 4°C and then stored in 70% ethanol at 4°C for assessment of osteovascular composition.

106 Stroke Procedure

107 Ischemic stroke was induced with the middle cerebral artery occlusion (MCAo) procedure
108 using aseptic technique [25,26,28]. Anesthesia was induced with 5% isoflurane in a 70:30 N_2:O_2
109 gas mixture, then maintained with about 2% isoflurane. Stroke was induced by occluding the
110 middle cerebral artery with a thin 6-0 nylon monofilament occluder with a silicon-coated tip
111 (Doccol Corporation, Redlands, CA) for 30 minutes. MCAo was monitored using LDF (moor
112 VMS-LDF, Moor Instruments Ltd, Axminster, UK) with a monofilament probe (VP10M200ST,
113 Moor Instruments), ensuring that cerebral blood flow was reduced by 80% relative to baseline and
114 maintained throughout the procedure. The sham procedure was the same as the stroke procedure
115 but without insertion of the occluder. For tibial perfusion, a small, 2-5 mm-long incision was made
116 over the proximal anteromedial side of the left tibia near the metaphysis, avoiding underlying soft
117 tissue and muscle. A small region of the periosteum was scraped away (about 0.5 mm^2), and a
118 needle probe (VP4 Needle Probe, Moor Instruments) was held firmly against the bone with a
119 micromanipulator (MM3-ALL, World Precision Instruments, Sarasota, FL). The severity of stroke
120 impairments was examined weekly following surgery by assessing sensorimotor function with
121 neuroscores [27].

122

123 Treadmill Exercise

124 Exercise groups were acclimated to the treadmill (Exer 3/6, Columbus Instruments,
125 Columbus, OH) for two days prior to and two days following (on recovery days 4-5) the stroke or
126 sham procedure. After acclimation, exercise groups performed a standard moderate treadmill
127 exercise regimen (12 m/min, 30 min, 5 days/wk, 5° incline), while sedentary groups were placed
128 on a stationary replica treadmill for a matched time period.

129 Bone Perfusion (Tibia)

130 During the four-week recovery period, intraosseous perfusion was measured weekly in
131 affected (left) and unaffected (right) proximal tibiae using laser Doppler flowmetry (Fig. 2A) [29].
132 LDF provides a functional measure of blood flow in long bones that is influenced by the amount
133 of blood vessels, blood flow velocity, blood vessel permeability, and blood vessel size [20]. We
134 previously showed that our modified, less invasive LDF procedure can be performed serially
135 without inducing inflammation or gait abnormalities [30]. Using the same method as during the
136 MCAo procedure, an incision was made over one tibia, the periosteum was gently removed, and
137 the LDF needle probe was placed firmly against bone with the micromanipulator. A 30-sec
138 measurement was recorded, the probe was removed and repositioned, and a second 30-sec
139 measurement was recorded. The procedure was repeated for the contralateral tibia. Each weekly
140 perfusion measurement was composed of the weighted mean of the two 30-sec long measurements
141 for that bone.

142

143 Osteovascular Structure (Femur)

144 Osteovascular structure was examined in the subset of affected and unaffected femora
145 stored in PBS using contrast-enhanced micro-computed tomography (CE-CT). Each femur was
146 cut in half transversely with a scalpel, and the distal halves were incubated in a 3.695 mmol/L
147 staining solution of hafnium-substituted Wells-Dawson polyoxometalate hydrate in 1 mL PBS for
148 48 hours at 4°C according to a previously described protocol [31]. Samples were scanned with a
149 phoenix nanotom® m (GE Measurement and Control Solutions, Wunstorf, Germany) using 60 kV
150 peak X-ray tube potential, 140 µA X-ray intensity, and 500-ms integration time, and scans were
151 reconstructed at an isotropic voxel size of 2 µm.

152 Blood vessel and adipocyte microstructure was assessed in a manually selected volume of
153 interest (VOI) that was 1.6-mm long (about 10% average femur length), starting from the distal
154 growth plate and extending proximally into the metaphysis, excluding cortical bone tissue, using
155 the CTAn software (Bruker MicroCT, Kontich, Belgium). Within this VOI, cancellous bone was
156 segmented, binarized via automatic 3D Otsu segmentation, and subtracted from the image, leaving
157 the marrow volume. A manual global thresholding method was used to segment blood vessels and
158 adipocytes. The vessel volume fraction (vessel volume/marrow volume, Ves.V/Ma.V, %), vessel
159 density (Ves.D, #/mm^3), distribution of vessel thickness (Ves.Th, µm), adipocyte volume fraction
160 (adipocyte volume/marrow volume, Ad.V/Ma.V, %), adipocyte density (Ad.D, #/mm^3), and
161 distribution of adipocyte thickness (Ad.Th, µm) were quantified using CTAn. Branching
162 parameters of the osteovascular network, including total number of branches, number of junctions,
163 number of triple points (e.g., junctions with three branches), and number of quadruple points (e.g.,
164 junctions with four branches), were quantified in BoneJ (FIJI v. 1.51n) [32,33]. The distribution
165 of distances between blood vessel surfaces and bone surfaces (Ves.S-BS distance) was calculated
166 in MATLAB® (R2018, The MathWorks, Natick, MA).
167
168 Osteovascular Composition (Tibia)
169 Osteovascular composition was examined using immunofluorescence confocal
170 microscopy in bone tissue sections from a subset of affected tibiae (n = 3 sham-sedentary, n = 2
171 sham-exercise, n = 5 stroke-sedentary, n = 4 stroke-exercise) labeled for markers of non-arterial
172 endothelial cells (EMCN) and endothelial cells in sinuses, arterioles, venules, and capillaries
173 (CD31) [23,34]. Blood vessels that are positive for both EMCN and CD31 (defined as *Type H*)
174 have been shown to regulate bone-vascular crosstalk and couple osteo- and angiogenesis in long

175 bones [24]. Samples were prepared and labeled using a previously described procedure [35],
176 producing 50-µm-thick longitudinal sections of the proximal tibial metaphysis labeled for EMCN
177 and CD31. Nuclear staining was performed with DAPI.

178 Immediately following staining, sections were imaged at 20X on a Zeiss Laser Scanning
179 Microscope 880 with Airyscan (Carl Zeiss Microscopy, Thornwood, NY), and the areas of CD31-
180 positive, EMCN-positive, and Type H vessels, relative to total area, were quantified in a
181 metaphyseal region of interest (ROI) equal to 10% of the tibia length. CD31-positive regions inside
182 the ROI were manually traced into masks in FIJI, while EMCN-positive regions were
183 automatically binarized with custom code in MATLAB®. The CD31 mask, EMCN mask, and the
184 intersection of both masks (Type H) were calculated in FIJI. Osteovascular composition
185 parameters were measured in two sections per bone, and the mean values were used for analysis.
186

187 Statistical Analyses

188 Statistical models were analyzed with SAS (SAS University Edition v. 9.4, SAS Institute
189 Inc., Cary, NC) with a significance level of 0.05. Statistical models were designed to determine
190 the following: 1) effect of ischemic stroke and exercise on intraosseous perfusion during stroke
191 recovery; 2) acute effect of ischemic stroke on intraosseous perfusion during surgery; 3) effect of
192 stroke and exercise on osteovascular structure and composition; and 4) whether stroke
193 differentially affects intraosseous perfusion or osteovascular structure in the affected vs.
194 unaffected limb.

195 For analysis #1, LDF measures of perfusion were compared between surgery and activity
196 groups at each timepoint and limb using a mixed hierarchical linear model (procedure GLIMMIX)
197 with interaction between all terms [36]. LDF was measured across four timepoints (Weeks 1-4) on

198 each limb of each mouse. Effect differences between surgery and activity groups were compared
199 within each timepoint (i.e., stroke-exercise vs. stroke-sedentary at Week 2) using least squares
200 means and Tukey-Kramer adjustments for multiple comparisons.

201 For analysis #2, the stability of the tibial perfusion measurements throughout the surgery
202 was examined using the slope of the 30-minute LDF measurement taken during the surgical
203 procedure. To determine if the slope for each group was different from zero, which would indicate
204 that the perfusion measurement varied and was not stable, an unpaired t-test was performed for the
205 sham group, and a Wilcoxon rank sum test was performed for the stroke group. Slopes were also
206 compared between the stroke and sham groups with a Wilcoxon two-sample test.

207 For analysis #3, distribution data from CE-CT (vessel thickness, blood vessel surface to
208 bone surface distance) were compared between surgery and activity groups using a mixed
209 hierarchical linear model (procedure GLIMMIX) with interaction between terms. Effect
210 differences were compared between groups within histogram bins (i.e., stroke-exercise vs. stroke-
211 sedentary within bin 'a') using least squares means with Tukey-Kramer adjustments for multiple
212 comparisons. All other CE-CT parameters (Ad.V/Ma.V, average Ad.Th, Ad.D, Ves.V/Ma.V,
213 average Ves.Th, Ves.D, branches, junctions, triple points, and quadruple points) were compared
214 between surgery and activity groups using a repeated measures factorial model (procedure
215 MIXED) but without the 'bin' repeated factor. Immunofluorescence parameters were compared
216 between surgery and activity groups using a standard two-factor general linear model (procedure
217 GLM) with interaction and Tukey adjustments for multiple comparisons.

218 For analysis #4, the same repeated measures models from analyses 1 and 3 were used, but
219 least squares means were compared between limbs within surgery group (i.e., affected vs.
220 unaffected side within the stroke group).

221 Immunofluorescence and LDF data during MCAo are presented as mean ± standard
222 deviation. Data analyzed using least squares means (repeated LDF measures, CE-CT data) are
223 presented as least squares mean ± 95% confidence interval. Repeated LDF and CE-CT data are
224 presented as the least squares mean for both limbs per mouse unless otherwise noted.
225
226 **Results**
227 Bone Perfusion
228 Tibial perfusion was reduced in both limbs for two weeks following stroke, with 23% lower
229 perfusion in the stroke groups relative to the sham groups at Week 1 ($p = 0.0064$) and 24% lower
230 perfusion at Week 2 ($p = 0.0061$), but perfusion levels were similar between surgery groups at
231 Week 3 ($p = 0.71$) and Week 4 ($p = 0.60$) (Fig. 2B). Perfusion was nearly greater in exercise
232 groups, relative to sedentary groups, at Week 2 (21%, main effect $p = 0.050$), primarily driven by
233 the nearly increased perfusion in stroke-exercise (30% relative to stroke-sedentary, $p = 0.054$), not
234 sham-exercise (relative to sham-sedentary, $p = 0.32$). Exercise did not affect perfusion in other
235 weeks ($p = 0.94$ Week 1, $p = 0.79$ Week 3, $p = 0.22$ Week 4). Compared to the unaffected tibia,
236 perfusion in the affected tibia was nearly decreased for the stroke group at Week 2 (21%, $p =$
237 0.055) but not in Week 1 ($p = 0.42$), Week 3 (16%, $p = 0.11$), or Week 4 ($p = 0.58$) (Fig. 2C).
238 Perfusion was similar between affected and unaffected limbs for the sham group at all timepoints
239 ($p = 0.61$-0.90).
240 During the surgeries (occluded for stroke, not occluded for sham), tibial perfusion
241 measurements remained stable throughout, with slopes that were not significantly different from
242 zero for either stroke ($p = 0.39$) or sham ($p = 0.14$). The slopes were similar between stroke (-
243 0.0063 ± 0.0415 PU/min) and sham (0.0049 ± 0.0106 PU/min) groups ($p = 0.98$). These results

244 demonstrate that cerebral ischemia does not directly impact blood supply to the tibia during the
245 occlusion, suggesting that any changes to osteovasculature during the recovery period result from
246 more systemic effects.
247
248 Osteovascular Structure
249 Blood vessel volume fraction in the distal femur was increased by 38% in the stroke groups
250 relative to sham ($p = 0.0061$) and decreased by 14% in the exercise groups relative to sedentary (p
251 $= 0.031$, Fig. 3A-B). Exercise mitigated the effect of stroke, with 17% lower Ves.V/Ma.V in
252 stroke-exercise than in stroke-sedentary ($p = 0.027$), but did not affect blood vessel volume fraction
253 in sham-exercise compared to sham-sedentary ($p = 0.20$, Fig. 3B). Neither stroke ($p = 0.74$) nor
254 exercise ($p = 0.24$) affected blood vessel density (stroke-exercise: 132.9 ± 215.8 mm^{-3}, stroke-
255 sedentary: 62.2 ± 305.2 mm^{-3}, sham-exercise: 188.2 ± 215.8 mm^{-3}, sham-sedentary: 54.1 ± 305.2
256 mm^{-3}). The vessel network was more branched following stroke, with 26% greater number of
257 branches ($p = 0.0089$, Fig. 4A), 27% more junctions ($p = 0.015$, Fig. 4B), 33% more triple points
258 ($p = 0.040$, Fig. 4C) and 43% more quadruple points ($p = 0.017$, Fig. 4D), for the stroke group
259 compared to sham. Exercise did not affect any of these network branching parameters.
260 Neither stroke ($p = 0.31$) nor exercise ($p = 0.84$) affected mean blood vessel thickness (Fig.
261 3C). However, the distribution of Ves.Th was shifted following stroke, with fewer small vessels
262 (6-22 μm thickness, $p = 0.029$ for 6-10 μm, $p = 0.033$ for 10-14 μm, $p = 0.019$ for 14-18 μm, $p =$
263 0.056 for 18-22 μm) and more larger vessels (greater than 66 μm thickness, $p = 0.010$) (Fig. 5A).
264 Exercise mitigated the stroke-induced increase in larger blood vessels ($p = 0.0032$ stroke-exercise
265 vs. stroke-sedentary), bringing vessel thickness for stroke-exercise to similar values as sham-
266 exercise ($p = 0.72$) (Fig. 5A). The proximity of blood vessels to bone surfaces was altered by both

267 stroke and exercise, as seen by the shifted distribution of Ves.S-BS distance (Fig. 5B). Compared
268 to sham, the stroke group had 38% fewer blood vessels positioned within 4 μm of bone surfaces
269 ($p = 0.041$), 19% fewer blood vessels positioned 4-8 μm from bone surfaces ($p = 0.0010$), and
270 16% more vessels positioned 52 μm or farther away from bone surfaces ($p = 0.036$). Exercise had
271 a similar effect as stroke, with 33% fewer blood vessels within 4 μm of bone surfaces ($p = 0.017$)
272 and 16% more vessels 52 μm or farther away from bone surfaces ($p = 0.036$) compared to
273 sedentary. The effect of stroke and exercise were driven primarily by changes in the stroke-
274 exercise group, which had significantly fewer vessels positioned within 4 μm and significantly
275 more vessels positioned farther than 52 μm from bone surfaces compared to all other groups (Fig.
276 5B).

277 Adipocyte microstructure was not significantly affected by stroke or exercise, with similar
278 values for adipocyte volume fraction, density, and thickness across groups (Table I). However,
279 adipocyte density was nearly increased for stroke-exercise relative to sham-exercise (109%, $p =$
280 0.086). Affected and unaffected side measurements were not significantly different in the stroke
281 or sham groups for any of the CE-CT parameters (vessel microstructure, vessel branching, or
282 adipocyte microstructure).

283

284 Osteovascular Composition

285 Neither stroke nor exercise affected the relative area of endomucin-expressing ($p = 0.43$
286 and $p = 0.54$, Fig. 6B) or CD31-expressing ($p = 0.18$ and $p = 0.11$, Fig. 6C) blood vessels in the
287 proximal tibial metaphysis of affected limbs. The relative area of Type H vessels expressing both
288 EMCN and CD31 (Fig. 6A) was nearly lower for exercise compared to sedentary (186%, $p =$
289 0.059, Fig. 6D) but was not significantly different between stroke and sham ($p = 0.20$).

290 **Discussion**

291 This study is the first to report the effects of ischemic stroke on osteovasculature. Middle
292 cerebral artery occlusion in mice was associated with increased blood vessel volume within the
293 distal femoral metaphysis, primarily due to increased vascular branching and a greater number of
294 larger vessels. These changes followed reduced perfusion in the proximal tibia for two weeks
295 following stroke, with relatively lower blood supply to the affected than unaffected bone in stroke
296 groups but not sham groups. Furthermore, the effects of stroke and exercise on the proximity of
297 vessels to bone surfaces were driven primarily by changes in the stroke-exercise group, yielding
298 fewer blood vessels near to bone surfaces. Because previous studies have shown that active sites
299 of remodeling are associated with increased concentration of capillaries within 50 μm of the
300 remodeling surface compared to non-remodeling bone surfaces [21], these changes to
301 osteovascular structure and function may play a role in bone loss in stroke patients.

302 Limb disuse via hindlimb suspension has also been shown to decrease bone perfusion in
303 rodents [37,38]. However, in our study, mice remained ambulatory following the mild to moderate
304 severity stroke with no alterations in limb coordination patterns [27], yet bone perfusion was still
305 decreased post-stroke, even in the stroke-exercise group. Together, these results suggest that the
306 osteovascular changes in this study primarily result from more systemic stroke effects rather than
307 from limb disuse. Future work with this induced stroke model may improve understanding about
308 the pathogenesis of skeletal fragility in stroke patients, in particular examining how osteovascular
309 structure and function may contribute.

310 In this study, stroke decreased functional blood supply within the proximal tibia for two
311 weeks. Perfusion was reduced in both limbs and tended to be lower in the affected side than in the
312 unaffected side during the second and third week of recovery, mimicking the differential decreases

313 in lower leg blood flow observed in previous studies of chronic stroke patients with mild-to-
314 moderate gait asymmetry [17,18]. The decreased perfusion post-stroke was transient, returning to
315 sham levels by the third week of recovery in all stroke groups. Exercise accelerated this recovery,
316 with perfusion in the stroke-exercise group returning to sham-sedentary levels by the second week,
317 indicating that moderate exercise may be a viable strategy for increasing intraosseous blood supply
318 following stroke. Although a number of studies in human stroke patients have shown increased
319 limb perfusion with exercise following stroke [18,39], this study is the first to demonstrate that
320 exercise restores perfusion for the microvasculature within bone, as well.

321 Perfusion measurements alone do not provide information about changes to the structure
322 or composition of the vascular network, since perfusion could be reduced through decreased
323 vascular density, increased vascular tone, reduced vessel diameter, decreased vascular
324 permeability, or lower blood velocity. Stroke increased osteovascular volume, thickness, and
325 branching in the distal femur by the end of the four-week recovery period. Considering the early
326 transient reductions in bone perfusion in the proximal tibia, the increased osteovascular volume
327 may be a compensatory response to offset perfusion deficits. However, a study examining the
328 progression of these changes over time, and at the same site, is needed to assess the relative timing.

329 Ischemic stroke is associated with many conditions that could contribute to the reduced
330 intraosseous perfusion observed, including increased vascular tone, increased vascular resistance,
331 or decreased vasodilation. Vascular tone, which constricts blood vessels and decreases perfusion,
332 was higher in cutaneous blood vessels in the paretic hands of patients with ischemic lesions [40]
333 and in denervated arteries in rabbit ears [41], suggesting that stroke-related damage to the central
334 nervous system may contribute to the reduced intraosseous perfusion. Stroke has been associated
335 with increased vascular elasticity (a measure of vascular resistance) in the forearm [15], and

336 resistance arteries in cutaneous blood vessels in the paretic arms of stroke patients were also less
337 responsive to exogenous acetylcholine-induced vasodilation [42], which would increase vascular
338 resistance. However, the effect of stroke on the arteries that supply bone are unknown, and future
339 studies are required to determine whether increased vessel volume and branching are
340 compensatory for changes to vascular tone, resistance, or sensitivity to vasodilators following
341 stroke within long bones. Exercise restored the stroke-related perfusion deficits by the second
342 week of recovery but also reduced osteovascular volume relative to stroke-sedentary. Moderate
343 aerobic endurance training decreased peripheral vascular resistance in rats [43] and increased
344 vasodilator bioavailability in the leg in humans [44], suggesting that the exercise-related perfusion
345 increases may result, at least in part, from improved vascular function. Interestingly, exercise
346 mitigated the stroke-related increases in intraosseous vessel volume, further supporting the idea
347 that the increased vessel volume could be a pathological compensatory response and does not
348 necessarily reflect improved vascular function.

349 Although stroke increased the amount of blood vessels in bone, the structure and
350 composition of the osteovasculature were also affected, which may contribute to bone loss
351 following stroke. The combination of stroke and exercise decreased the relative number of blood
352 vessels near bone surfaces, which have been shown to be associated with sites of active bone
353 remodeling [21,22,45]. Exercise, in mitigating increased blood vessel volume post-stroke, may
354 have also reduced the number of branches in close contact with bone surfaces. Since exercise did
355 not reduce vessel-bone distance in the sham-exercise group, and since stroke did not decrease
356 vessel-bone distance in the stroke-sedentary group, the combined effect of exercise and stroke may
357 compound the detrimental changes in vessel proximity to bone surfaces. Although the relative area
358 of Type H endothelia was not affected by stroke in the tibia, stroke shifted the distribution of blood

359 vessel diameter in the femur, decreasing the amount of vessels between 6-22 μm in diameter,
360 which matches the size of Type H capillaries known to regulate osteogenesis [23]. Stroke causes
361 chronic inflammation [46], which stimulates angiogenesis [47] and thus may be responsible for
362 the increased vascular volume and branching following stroke, but inflammation also dysregulates
363 Notch signaling [48], the mechanism by which Type H capillaries regulate bone modeling [23,24].
364 Conversely, exercise nearly lowered the relative area of Type H endothelia in the proximal tibia
365 in both sham and stroke groups but did not affect the number of branches or vessel thickness
366 distribution in the distal femur. The reduction in relative area of Type H endothelial vessels could
367 be due to increased hypoxia-inducible factor (HIF) signaling, which, like Notch, is responsible for
368 Type H activity [24]. Since HIF is released by tissues experiencing hypoxia, HIF in the marrow
369 space may be increased with exercise following stroke if perfusion is negatively affected, and less
370 oxygen and fewer nutrients are able to reach bone tissue. Although some HIF signaling helps
371 recruit osteoblasts [24], compromised bone blood flow restricts oxygen availability to bone cells,
372 stimulating bone resorption [49], and reduced Type H activity could decrease osteogenesis [45].
373 Despite the increased amount of osteovasculature, the reduction in vessel-bone proximity,
374 resulting primarily from loss of small vessels, may explain the lack of exercise-induced gains in
375 bone microstructure following stroke, which we found in the same region using the same bones as
376 in this study [27].

377 In this study, we extended previous clinical findings that limb perfusion is reduced
378 following ischemic stroke and demonstrated for the first time, using a mouse model, that
379 intraosseous perfusion is also reduced during early stroke recovery, particularly in the affected
380 limb, and notably even in the absence of limb disuse. These functional deficits occurred in
381 conjunction with changes in osteovascular structure, including potentially compensatory increases

382 in vascular volume, branching, and the number of larger vessels. Further, although exercise
383 mitigated the negative effects of stroke on bone perfusion, the combination of stroke and exercise
384 altered the vessel proximity to bone to a less osteogenic arrangement with fewer small vessels
385 located near bone. These findings suggest that exercise like this moderate treadmill regime may
386 not be beneficial for osteovascular structure, although more studies are needed to examine if these
387 effects extend to other exercise therapies or rehabilitation strategies. Examining potential
388 mechanisms for these changes in osteovascular structure and function following stroke may
389 provide insight for mitigating skeletal fragility in human stroke patients.

Acknowledgments

We thank Dr. Eva Johannes and Dr. Mariusz Zareba for confocal microscopy support; and Dr. Consuelo Arellano for statistical consulting. This work was performed in part at the Cellular and Molecular Imaging Facility (CMIF) at North Carolina State University, which is supported by the State of North Carolina and the National Science Foundation.

Sources of Funding

Research reported in this publication was supported by the Eunice Kennedy Shriver National Institute of Child Health and Human Development (NICHD) of the NIH under award number K12HD073945 and by the American Heart Association (AHA) under award number 7GRNT33710007. The content is solely the responsibility of the authors and does not necessarily represent the official views of the NIH.

Disclosures

The authors have nothing to disclose.

References

[1] E.J. Benjamin, P. Muntner, A. Alonso, M.S. Bittencourt, C.W. Callaway, A.P. Carson, A.M. Chamberlain, A.R. Chang, S. Cheng, S.R. Das, F.N. Delling, L. Djousse, M.S.V. Elkind, J.F. Ferguson, M. Fornage, L.C. Jordan, S.S. Khan, B.M. Kissela, K.L. Knutson, T.W. Kwan, D.T. Lackland, T.T. Lewis, J.H. Lichtman, C.T. Longenecker, M.S. Loop, P.L. Lutsey, S.S. Martin, K. Matsushita, A.E. Moran, M.E. Mussolino, M. O'Flaherty, A. Pandey, A.M. Perak, W.D. Rosamond, G.A. Roth, U.K.A. Sampson, G.M. Satou, E.B. Schroeder, S.H. Shah, N.L. Spartano, A. Stokes, D.L. Tirschwell, C.W. Tsao, M.P. Turakhia, L.B. VanWagner, J.T. Wilkins, S.S. Wong, S.S. Virani, American Heart Association Council on Epidemiology and Prevention Statistics Committee and Stroke Statistics Subcommittee, Heart Disease and Stroke Statistics-2019 Update: A Report From the American Heart Association, Circulation. 139 (2019) e56–e528. doi:10.1161/CIR.0000000000000659.

[2] J. Kanis, A. Oden, O. Johnell, Acute and Long-Term Increase in Fracture Risk After Hospitalization for Stroke, Stroke. 32 (2001) 702–706. doi:10.1161/01.STR.32.3.702.

[3] L. Jørgensen, B.K. Jacobsen, T. Wilsgaard, J.H. Magnus, Walking after Stroke: Does It Matter? Changes in Bone Mineral Density Within the First 12 Months after Stroke. A Longitudinal Study, Osteoporos. Int. 11 (2000) 381–387. doi:10.1007/s001980070103.

[4] L. Jørgensen, B.K. Jacobsen, Functional status of the paretic arm affects the loss of bone mineral in the proximal humerus after stroke: a 1-year prospective study, Calcif. Tissue Int. 68 (2001) 11–15. doi:10.1007/s002230001165.

[5] A. Ramnemark, L. Nyberg, B. Borssén, T. Olsson, Y. Gustafson, Fractures after Stroke, Osteoporos. Int. 8 (1998) 92–95. doi:10.1007/s001980050053.

428 [6] A. Ramnemark, L. Nyberg, R. Lorentzon, U. Englund, Y. Gustafson, Progressive
429 Hemiosteoporosis on the Paretic Side and Increased Bone Mineral Density in the Nonparetic
430 Arm the First Year after Severe Stroke, Osteoporos. Int. 9 (1999) 269–275.
431 doi:10.1007/s001980050147.
432 [7] A. Fisher, W. Srikusalanukul, M. Davis, P. Smith, Poststroke Hip Fracture: Prevalence,
433 Clinical Characteristics, Mineral-Bone Metabolism, Outcomes, and Gaps in Prevention,
434 Stroke Res. Treat. 2013 (2013). doi:10.1155/2013/641943.
435 [8] G.S. Beaupré, H.L. Lew, Bone-Density Changes After Stroke, Am. J. Phys. Med. Rehabil.
436 85 (2006) 464–472. doi:10.1097/01.phm.0000214275.69286.7a.
437 [9] H.M. Frost, Bone's Mechanostat: A 2003 Update, Anat. Rec. A. Discov. Mol. Cell. Evol.
438 Biol. 275A (2003) 1081–1101. doi:10.1002/ar.a.10119.
439 [10] J.J. Eng, M.Y.C. Pang, M.C. Ashe, Balance, falls, and bone health : role of exercise in
440 reducing fracture risk after stroke, J. Rehabil. Res. Dev. 45 (2008) 297–314.
441 [11] M.Y.C. Pang, R.W.K. Lau, The Effects of Treadmill Exercise Training on Hip Bone
442 Density and Tibial Bone Geometry in Stroke Survivors: A Pilot Study, Neurorehabil. Neural
443 Repair. 24 (2010) 368–376. doi:10.1177/1545968309353326.
444 [12] R.P.V. Peppen, G. Kwakkel, S. Wood-Dauphinee, H.J. Hendriks, P.J.V. der Wees, J.
445 Dekker, The impact of physical therapy on functional outcomes after stroke: what's the
446 evidence?, Clin. Rehabil. 18 (2004) 833–862. doi:10.1191/0269215504cr843oa.
447 [13] K. Borschmann, M.Y.C. Pang, S. Iuliano, L. Churilov, A. Brodtmann, E.I. Ekinci, J.
448 Bernhardt, Changes to volumetric bone mineral density and bone strength after stroke: a
449 prospective study, Int. J. Stroke Off. J. Int. Stroke Soc. 10 (2015) 396–399.
450 doi:10.1111/ijs.12228.

451 [14] A.M. Weatherholt, K.G. Avin, A.L. Hurd, J.L. Cox, S.T. Marberry, B.G. Santoni, S.J.
452 Warden, Peripheral quantitative computed tomography (pQCT) predicts humeral diaphysis
453 torsional mechanical properties with good short-term precision, J. Clin. Densitom. Off. J. Int.
454 Soc. Clin. Densitom. 18 (2015) 551–559. doi:10.1016/j.jocd.2014.10.002.
455 [15] M.Y.C. Pang, F.Z.H. Yang, A.Y.M. Jones, Vascular Elasticity and Grip Strength Are
456 Associated With Bone Health of the Hemiparetic Radius in People With Chronic Stroke:
457 Implications for Rehabilitation, Phys. Ther. 93 (2013) 774–785. doi:10.2522/ptj.20120378.
458 [16] S. Stegen, G. Carmeliet, The skeletal vascular system – Breathing life into bone tissue,
459 Bone. 115 (2018) 50–58. doi:10.1016/j.bone.2017.08.022.
460 [17] F.M. Ivey, A.W. Gardner, C.L. Dobrovolny, R.F. Macko, Unilateral Impairment of Leg
461 Blood Flow in Chronic Stroke Patients, Cerebrovasc. Dis. Basel. 18 (2004) 283–9.
462 [18] F.M. Ivey, C.E. Hafer-Macko, A.S. Ryan, R.F. Macko, Impaired Leg Vasodilatory
463 Function After Stroke: Adaptations With Treadmill Exercise Training, Stroke. 41 (2010)
464 2913–2917. doi:10.1161/STROKEAHA.110.599977.
465 [19] J. Reeve, M. Arlot, R. Wootton, C. Edouard, M. Tellez, R. Hesp, J.R. Green, P.J.
466 Meunier, Skeletal Blood Flow, Iliac Histomorphometry, and Strontium Kinetics in
467 Osteoporosis: A Relationship Between Blood Flow and Corrected Apposition Rate, J. Clin.
468 Endocrinol. Metab. 66 (1988) 1124–1131. doi:10.1210/jcem-66-6-1124.
469 [20] J.F. Griffith, D.K. Yeung, P.H. Tsang, K.C. Choi, T.C. Kwok, A.T. Ahuja, K.S. Leung,
470 P.C. Leung, Compromised Bone Marrow Perfusion in Osteoporosis, J. Bone Miner. Res. 23
471 (2008) 1068–1075. doi:10.1359/jbmr.080233.

472 [21] H.B. Kristensen, T.L. Andersen, N. Marcussen, L. Rolighed, J.-M. Delaisse, Increased
473 presence of capillaries next to remodeling sites in adult human cancellous bone, J. Bone
474 Miner. Res. 28 (2013) 574–585. doi:10.1002/jbmr.1760.
475 [22] R. Prisby, A. Guignandon, A. Vanden-Bossche, F. Mac-Way, M.-T. Linossier, M.
476 Thomas, N. Laroche, L. Malaval, M. Langer, Z.-A. Peter, F. Peyrin, L. Vico, M.-H. Lafage-
477 Proust, Intermittent PTH(1–84) is osteoanabolic but not osteoangiogenic and relocates bone
478 marrow blood vessels closer to bone-forming sites, J. Bone Miner. Res. 26 (2011) 2583–
479 2596. doi:10.1002/jbmr.459.
480 [23] S.K. Ramasamy, A.P. Kusumbe, L. Wang, R.H. Adams, Endothelial Notch activity
481 promotes angiogenesis and osteogenesis in bone, Nature. 507 (2014) 376–380.
482 doi:10.1038/nature13146.
483 [24] A.P. Kusumbe, S.K. Ramasamy, R.H. Adams, Coupling of angiogenesis and
484 osteogenesis by a specific vessel subtype in bone, Nature. 507 (2014) 323–328.
485 doi:10.1038/nature13145.
486 [25] J. Koizumi, Y. Yoshida, T. Nakazawa, G. Ooneda, Experimental studies of ischemic
487 brain edema, I: a new experimental model of cerebral embolism in rats in which recirculation
488 can be introduced in the ischemic area, Jnp J Stroke. 8 (1986).
489 [26] E.Z. Longa, P.R. Weinstein, S. Carlson, R. Cummins, Reversible middle cerebral artery
490 occlusion without craniectomy in rats., Stroke. 20 (1989) 84–91.
491 doi:10.1161/01.STR.20.1.84.
492 [27] N.J. Hanne, A.J. Steward, M.R. Sessions, H.L. Thornburg, H. Sheng, J.H. Cole, Stroke
493 prevents exercise-induced gains in bone microstructure but not composition in mice,
494 BioRxiv. (2019) 708388. doi:10.1101/708388.

495 [28] H. Sakai, H. Sheng, R.B. Yates, K. Ishida, R.D. Pearlstein, D.S. Warner, Isoflurane
496 provides long-term protection against focal cerebral ischemia in the rat, Anesthesiology. 106
497 (2007) 92–99; discussion 8-10.
498 [29] N.J. Hanne, E.D. Easter, S. Stangeland-Molo, J.H. Cole, A Minimally Invasive
499 Technique for Serial Intraosseous Perfusion Measurements in the Murine Tibia Using Laser
500 Doppler Flowmetry, BioRxiv. (2019) 708453. doi:10.1101/708453.
501 [30] N.J. Hanne, E.D. Easter, J.H. Cole, Validating Minimally Invasive Laser Doppler
502 Flowmetry for Serial Bone Perfusion Measurements in Mice, BioRxiv. (2019) 708412.
503 doi:10.1101/708412.
504 [31] G. Kerckhofs, S. Stegen, N. van Gastel, A. Sap, G. Falgayrac, G. Penel, M. Durand, F.P.
505 Luyten, L. Geris, K. Vandamme, T. Parac-Vogt, G. Carmeliet, Simultaneous three-
506 dimensional visualization of mineralized and soft skeletal tissues by a novel microCT
507 contrast agent with polyoxometalate structure, Biomaterials. 159 (2018) 1–12.
508 doi:10.1016/j.biomaterials.2017.12.016.
509 [32] M. Doube, M.M. Kłosowski, I. Arganda-Carreras, F.P. Cordelières, R.P. Dougherty, J.S.
510 Jackson, B. Schmid, J.R. Hutchinson, S.J. Shefelbine, BoneJ: Free and extensible bone
511 image analysis in ImageJ, Bone. 47 (2010) 1076–1079. doi:10.1016/j.bone.2010.08.023.
512 [33] J. Schindelin, I. Arganda-Carreras, E. Frise, V. Kaynig, M. Longair, T. Pietzsch, S.
513 Preibisch, C. Rueden, S. Saalfeld, B. Schmid, J.-Y. Tinevez, D.J. White, V. Hartenstein, K.
514 Eliceiri, P. Tomancak, A. Cardona, Fiji: an open-source platform for biological-image
515 analysis, Nat. Methods. 9 (2012) 676–682. doi:10.1038/nmeth.2019.
516 [34] M.P. Pusztaszeri, W. Seelentag, F.T. Bosman, Immunohistochemical expression of
517 endothelial markers CD31, CD34, von Willebrand factor, and Fli-1 in normal human tissues,

518 J. Histochem. Cytochem. Off. J. Histochem. Soc. 54 (2006) 385–395.
519 doi:10.1369/jhc.4A6514.2005.
520 [35] A.P. Kusumbe, S.K. Ramasamy, A. Starsichova, R.H. Adams, Sample preparation for
521 high-resolution 3D confocal imaging of mouse skeletal tissue, Nat. Protoc. Lond. 10 (2015)
522 1904–1914. doi:http://dx.doi.org.prox.lib.ncsu.edu/10.1038/nprot.2015.125.
523 [36] R.C. Littell, ed., SAS for mixed models, 2nd ed, SAS Institute, Inc, Cary, N.C, 2006.
524 [37] J.N. Stabley, R.D. Prisby, B.J. Behnke, M.D. Delp, Chronic skeletal unloading of the rat
525 femur: Mechanisms and functional consequences of vascular remodeling, Bone. 57 (2013)
526 355–360. doi:10.1016/j.bone.2013.09.003.
527 [38] P.N. Colleran, M.K. Wilkerson, S.A. Bloomfield, L.J. Suva, R.T. Turner, M.D. Delp,
528 Alterations in skeletal perfusion with simulated microgravity: a possible mechanism for bone
529 remodeling, J. Appl. Physiol. 89 (2000) 1046–1054.
530 [39] Billinger Sandra A., Gajewski Byron J., Guo Lisa X., Kluding Patricia M., Single Limb
531 Exercise Induces Femoral Artery Remodeling and Improves Blood Flow in the Hemiparetic
532 Leg Poststroke, Stroke. 40 (2009) 3086–3090. doi:10.1161/STROKEAHA.109.550889.
533 [40] A.G. Herbaut, J.D. Cole, E.M. Sedgwick, A cerebral hemisphere influence on cutaneous
534 vasomotor reflexes in humans., J. Neurol. Neurosurg. Psychiatry. 53 (1990) 118–120.
535 [41] R.D. Bevan, A. Clementson, E. Joyce, J.A. Bevan, Sympathetic denervation of resistance
536 arteries increases contraction and decreases relaxation to flow, Am. J. Physiol.-Heart Circ.
537 Physiol. 264 (1993) H490–H494. doi:10.1152/ajpheart.1993.264.2.H490.
538 [42] J.-S. Wang, C.F. Yang, M.-Y. Liaw, M.-K. Wong, Suppressed cutaneous endothelial
539 vascular control and hemodynamic changes in paretic extremities with edema in the

540 extremities of patients with hemiplegia, Arch. Phys. Med. Rehabil. 83 (2002) 1017–1023.
541 doi:10.1053/apmr.2002.33235.
542 [43] M.K. Karhunen, M.P. Rämö, R. Kettunen, L. Hirvonen, The cardiovascular effects of
543 deconditioning after endurance training in rats, Acta Physiol. Scand. 133 (1988) 307–314.
544 doi:10.1111/j.1748-1716.1988.tb08412.x.
545 [44] J. Sugawara, H. Komine, K. Hayashi, M. Yoshizawa, T. Otsuki, N. Shimojo, T.
546 Miyauchi, T. Yokoi, S. Maeda, H. Tanaka, Systemic α-adrenergic and nitric oxide inhibition
547 on basal limb blood flow: effects of endurance training in middle-aged and older adults, Am.
548 J. Physiol.-Heart Circ. Physiol. 293 (2007) H1466–H1472. doi:10.1152/ajpheart.00273.2007.
549 [45] T.L. Andersen, T.E. Sondergaard, K.E. Skorzynska, F. Dagnaes-Hansen, T.L. Plesner,
550 E.M. Hauge, T. Plesner, J.-M. Delaisse, A Physical Mechanism for Coupling Bone
551 Resorption and Formation in Adult Human Bone, Am. J. Pathol. 174 (2009) 239–247.
552 doi:10.2353/ajpath.2009.080627.
553 [46] K.L. Lambertsen, K. Biber, B. Finsen, Inflammatory cytokines in experimental and
554 human stroke, J. Cereb. Blood Flow Metab. 32 (2012) 1677–1698.
555 doi:10.1038/jcbfm.2012.88.
556 [47] C. Costa, J. Incio, R. Soares, Angiogenesis and chronic inflammation: cause or
557 consequence?, Angiogenesis. 10 (2007) 149–166. doi:10.1007/s10456-007-9074-0.
558 [48] T. Quillard, J. Devallière, S. Coupel, B. Charreau, Inflammation dysregulates Notch
559 signaling in endothelial cells: Implication of Notch2 and Notch4 to endothelial dysfunction,
560 Biochem. Pharmacol. 80 (2010) 2032–2041. doi:10.1016/j.bcp.2010.07.010.

561 [49] T.R. Arnett, D.C. Gibbons, J.C. Utting, I.R. Orriss, A. Hoebertz, M. Rosendaal, S.
562 Meghji, Hypoxia is a major stimulator of osteoclast formation and bone resorption, J. Cell.
563 Physiol. 196 (2003) 2–8. doi:10.1002/jcp.10321.
564

Tables

Table I. Adipocyte Microstructure in the Distal Femoral Metaphysis

Trait	Sham		Stroke	
	Sedentary	**Exercise**	**Sedentary**	**Exercise**
Ad.V/Ma.V (%)	0.15 ± 0.77	0.16 ± 0.55	0.15 ± 0.77	0.45 ± 0.55
Ad.D (#/mm^3)	127.7 ± 166.4	113.5 ± 117.7	118.4 ± 166.4	237.0 ± 117.7*
Ad.Th (μm)	20.5 ± 10.3	20.7 ± 7.3	20.2 ± 10.3	23.1 ± 7.3

least squares mean ± 95% confidence interval

*: $p < 0.10$ stroke-exercise vs. sham-exercise

Figures and Legends

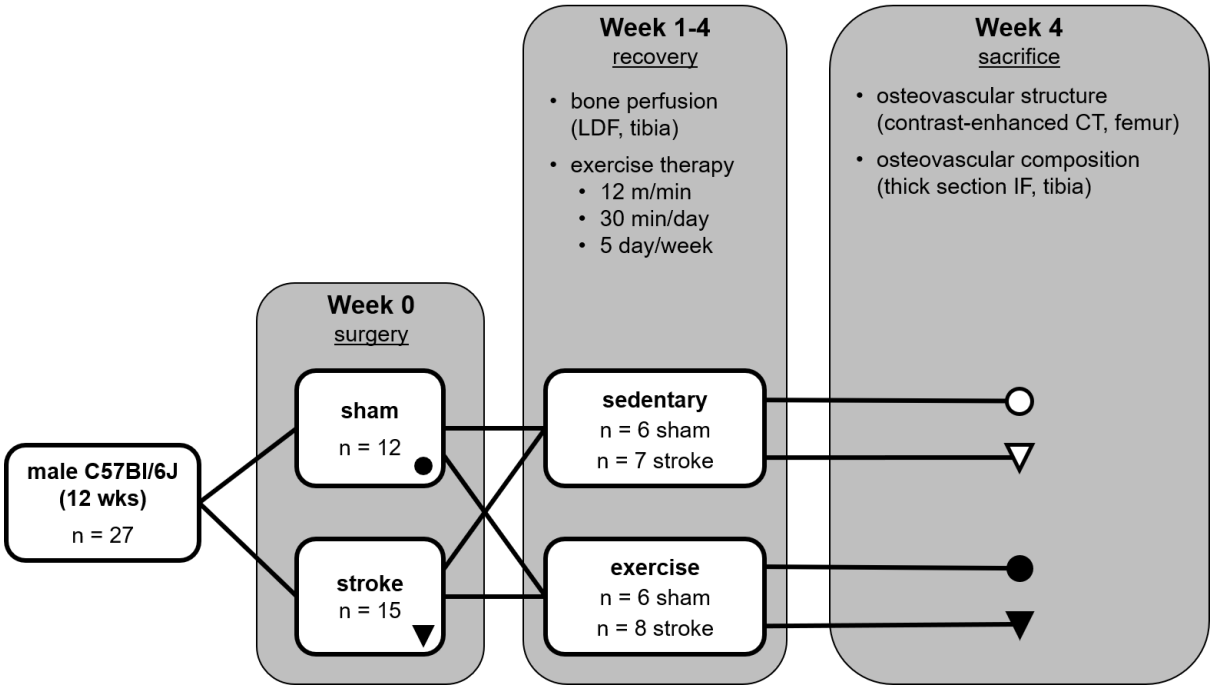

Figure 1. Study design. Mice received stroke or sham surgery, followed by four weeks of treadmill or sedentary activity. Intraosseous perfusion was measured weekly during recovery in affected and unaffected tibiae with laser Doppler flowmetry (LDF). After sacrifice, osteovascular structure and composition were characterized with contract-enhanced computed tomography (CT) and immunofluorescence (IF) microscopy.

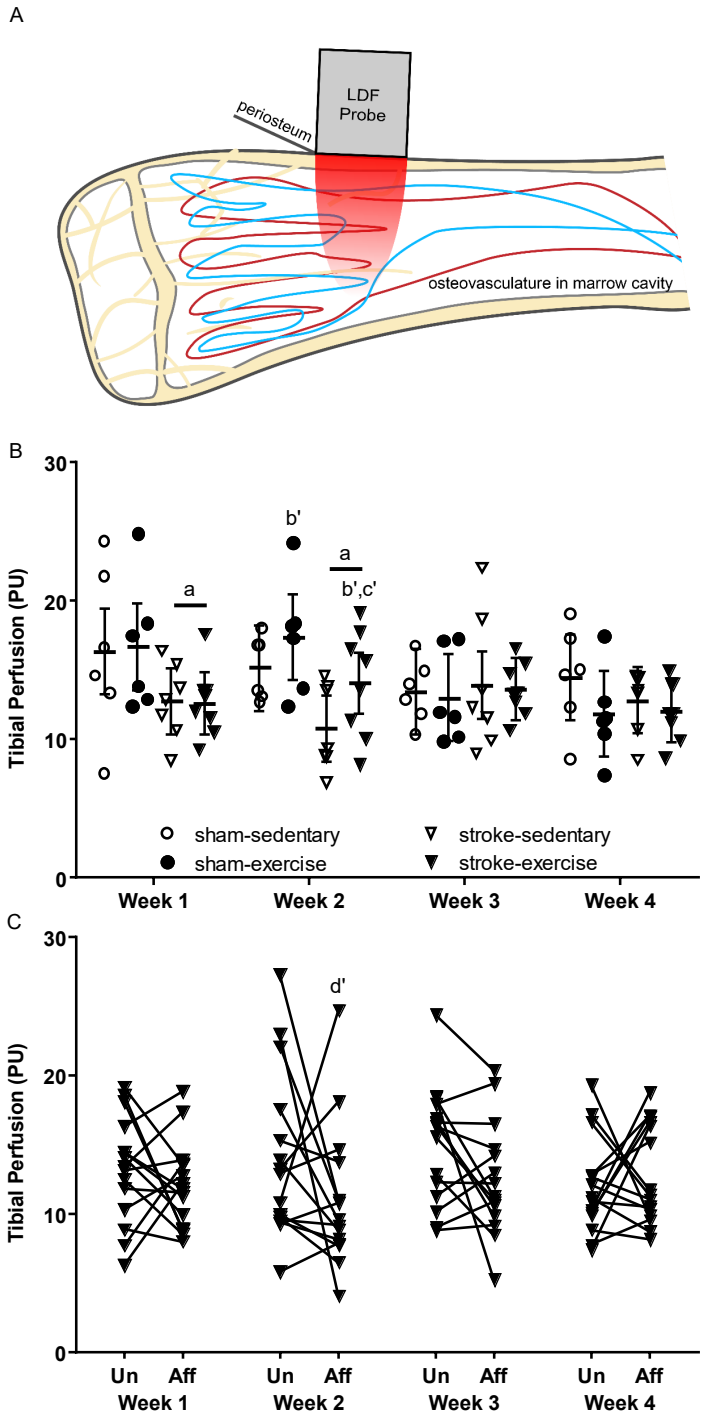

Figure 2. A) Intraosseous perfusion in proximal tibiae measured by laser Doppler flowmetry. B) Perfusion decreased in both limbs at Weeks 1 and 2 post-stroke and was increased with exercise at Week 2 (least squares mean ± 95% confidence interval across both limbs). C) Comparing limbs for stroke, perfusion was nearly decreased in the affected (Aff) relative to unaffected (Un) limb during Week 2. a: $p < 0.05$ stroke vs. sham (main effect); b′: $p < 0.1$ exercise vs. sedentary (main effect); c′: $p < 0.1$ stroke-exercise vs. stroke-sedentary; d′: $p < 0.1$ Aff vs. Un limb within stroke group.

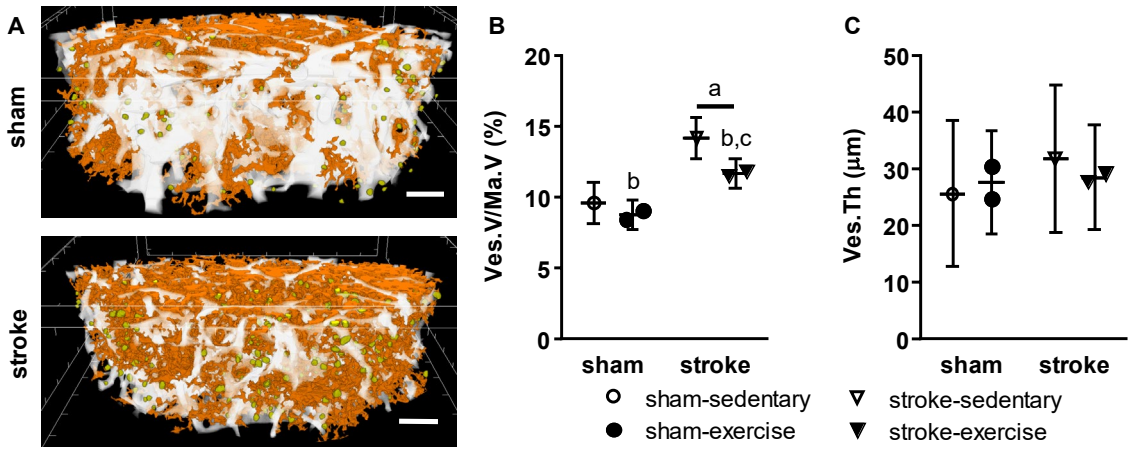

Figure 3. A) Osteovascular structure in the distal femoral metaphysis. B) Blood vessel volume fraction was increased with stroke, while exercise mitigated the effect of stroke. C) Mean vessel thickness was not altered by stroke or exercise. a: $p < 0.05$ stroke vs. sham (main effect); b: $p < 0.05$ exercise vs. sedentary (main effect); c: $p < 0.05$ stroke-exercise vs. stroke-sedentary.

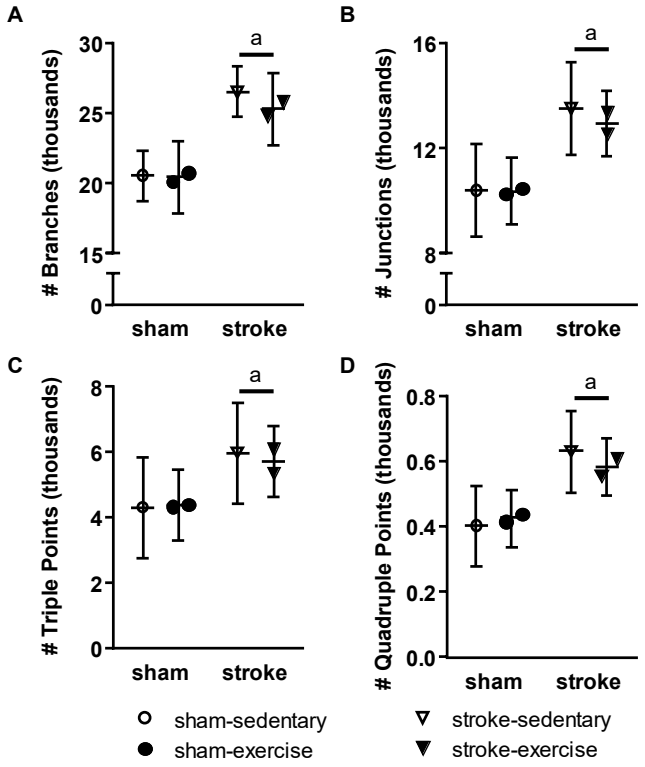

Figure 4. Osteovascular network in the distal femoral metaphysis. A) Vascular branching, B) number of junctions, C) number of triple points, and D) number of quadruple points were increased with stroke. a: $p < 0.05$ stroke vs. sham (main effect); a′: $p < 0.10$ stroke vs. sham (main effect).

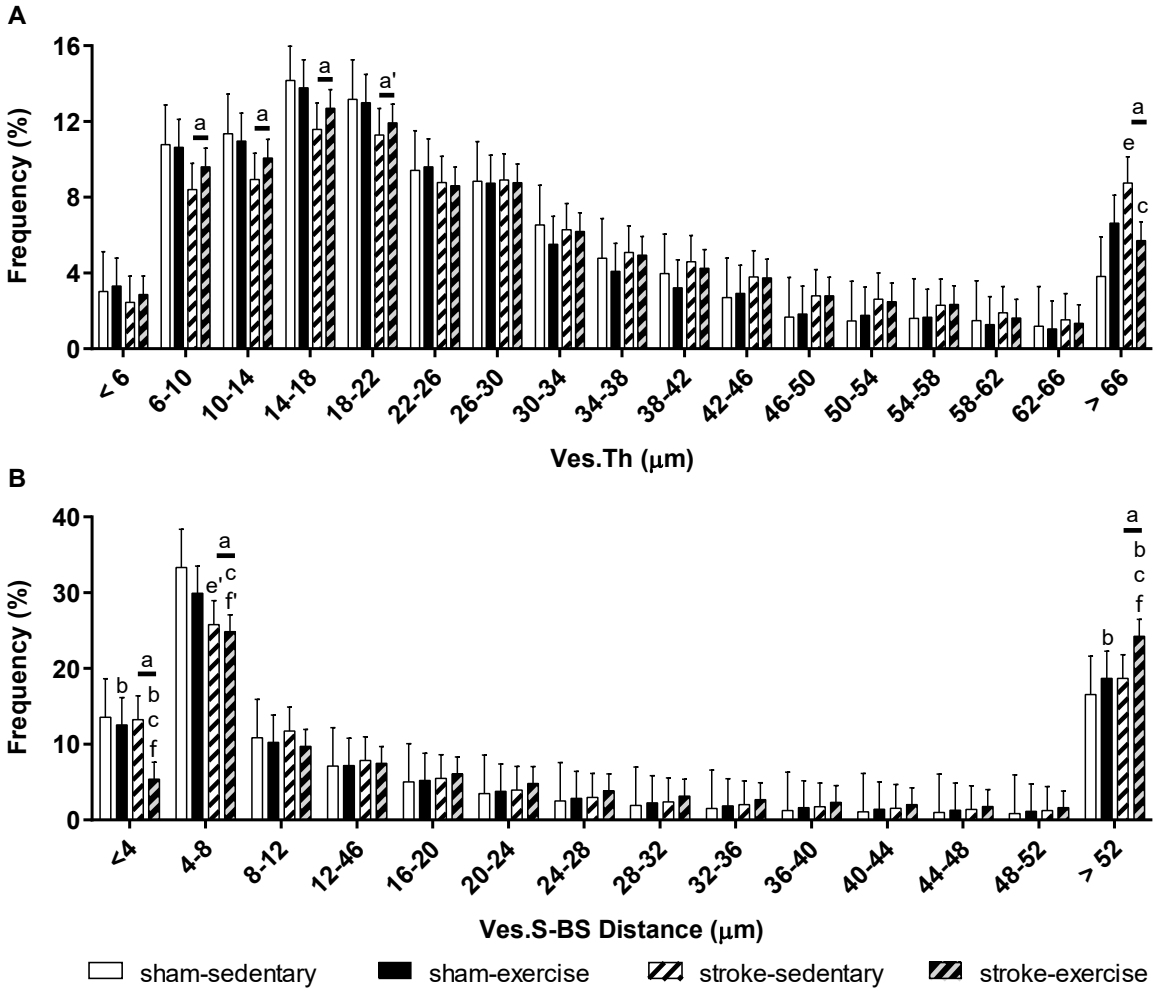

Figure 5. Osteovascular arrangement in the distal femoral metaphysis. A) Distribution of vessel thickness was shifted with stroke, with fewer smaller vessels and more larger vessels. Exercise mitigated the stroke-induced increase in large vessels. B) Both stroke and exercise reduced the relative number of blood vessels nearer to bone surfaces and increased the number farther from bone surfaces, especially for stroke-exercise. a: $p < 0.05$ stroke vs. sham (main effect); a′: $p < 0.10$ stroke vs. sham (main effect); b: $p < 0.05$ exercise vs. sedentary (main effect); c: $p < 0.05$ stroke-exercise vs. stroke-sedentary; e: $p < 0.05$ stroke-sedentary vs. sham-sedentary; e': $p < 0.10$ stroke-sedentary vs. sham-sedentary; f: $p < 0.05$ stroke-exercise vs. sham-exercise; f': $p < 0.10$ stroke-exercise vs. sham-exercise.

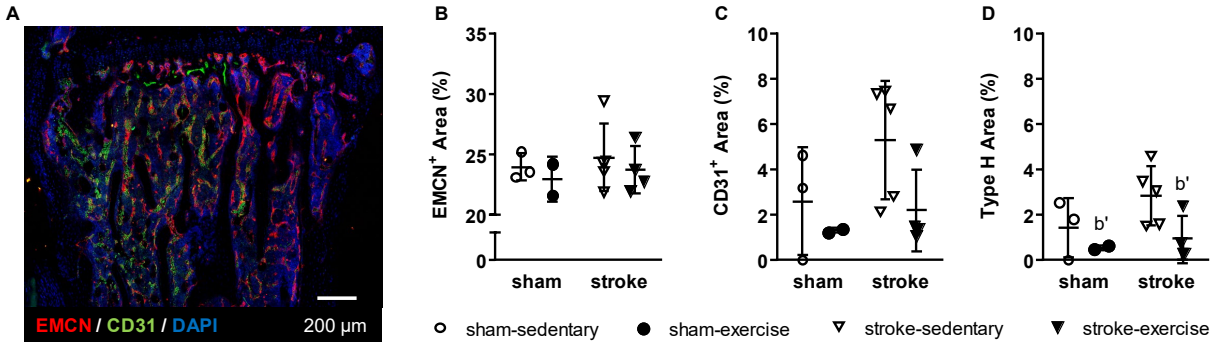

Figure 6. A) Representative longitudinal section in proximal tibia metaphysis, showing osteovascular composition with immunofluorescence. B) Endomucin $(EMCN)^+$ and C) $CD31^+$ areas were unaffected by stroke or exercise. D) Relative area of Type H endothelial cells ($EMCN^+$ and $CD31^+$) was nearly reduced by exercise. b′: $p < 0.1$ exercise vs. sedentary (main effect).

SUPPLEMENTAL MATERIAL

Detailed Methods

Stroke Procedure

Following 6-8 hours of fasting, ischemic stroke was induced with the middle cerebral artery occlusion (MCAo) procedure using aseptic technique [1–3]. Anesthesia was induced with 5% isoflurane in a 70:30 N_2:O_2 gas mixture, then maintained with about 2% isoflurane. Once mice were anesthetized, fur was shaved over the three incision sites at the anterior neck (for MCAo and sham procedures), the anterior region of the temporalis muscle (for skull LDF probe), and the left proximal tibia (for bone LDF probe). Mice were placed supine on a heated pad, and rectal temperature was maintained at 37°C throughout the procedure (TCAT-2DF, Physitemp Instruments, LLC, Clifton, NJ). LDF was used to monitor both cerebral blood flow (CBF) and perfusion in the proximal tibia using a 785-nm light source (moorVMS-LDF, Moor Instruments Ltd, Axminster, UK). For CBF, a small, 2-5 mm-long incision was made over the right temporal bone, and a monofilament probe (VP10M200ST, Moor Instruments Ltd) was affixed directly to the skull behind the temporalis muscle with cyanoacrylate glue. CBF was recorded with a cutoff frequency of 15 kHz selected for the low-pass filter, along with the automatically applied 20-Hz high-pass filter. For tibial perfusion, a small, 2-5 mm-long incision was made over the proximal anteromedial side of the left tibia near the metaphysis, avoiding underlying soft tissue and muscle. A small region of the periosteum was scraped away (about 0.5 mm^2), and a needle probe (VP4 Needle Probe, Moor Instruments Ltd) was held firmly against the bone with a micromanipulator (MM3-ALL, World Precision Instruments, Sarasota, FL). Tibial intraosseous perfusion was recorded with a cutoff frequency of 3 kHz selected for the low-pass filter and the automatic 20-Hz high-pass filter.

For the stroke or sham surgery, an incision was made over the neck midline, and the right common carotid artery (CCA), external carotid artery (ECA), and internal carotid artery (ICA) were exposed. In the sham group, saline was added to the neck incision to prevent tissue from drying out, CBF was monitored, and tibial perfusion was recorded for 30 minutes. In the stroke group, temporary ligations were made to the CCA and ICA, while two permanent ligations were made to the ECA, and the vessel was cut between them. Baseline CBF values were collected by loosening the CCA ligation for 2 minutes. The CCA ligation was then retightened, and a thin 6-0 nylon monofilament occluder with a silicon-coated tip (Doccol Corporation, Redlands, CA) was passed through the ECA to the ICA and MCA origin until an 80% reduction in CBF relative to baseline was noted and maintained. The size of the silicon coating was selected based on body mass, per the manufacturer's instructions, and either a 1-2 or 2-3 mm long, 0.20-0.24 mm diameter coating was selected. Saline was added to the incision to prevent tissue from drying out. The occluding filament was left in place for 30 minutes, and tibial perfusion was recorded. After 30 minutes, the occluder was gently retracted, the ECA was permanently ligated, and temporary ligations were removed. For both sham and stroke procedures, the LDF probes were removed, and an intraincisional injection of bupivacaine (2 mg/kg, Marcaine, Hospira, Lake Forest, IL) was administered to the neck. The neck and skull incisions were sutured closed, and the hindlimb incision was closed with tissue adhesive (VetBond™, 3M Company, St. Paul, MN). Triple antibiotic ointment and 4% lidocaine cream were applied to all incision sites, and a subcutaneous injection of carprofen (7 mg/kg, Rimadyl, Zoetis, Parsippany, NJ) was administered. Bupivacaine was administered via subcutaneous injection for the first two days of recovery. The severity of stroke impairments was examined weekly following surgery by assessing sensorimotor function with neuroscores [4].

Bone Perfusion (Tibia)

During the four-week recovery period, intraosseous perfusion was measured weekly in affected (left) and unaffected (right) proximal tibiae using laser Doppler flowmetry (Fig. 2A) [5]. LDF provides a functional measure of blood flow in long bones that is influenced by the amount of blood vessels, blood flow velocity, blood vessel permeability, and blood vessel size [6]. We previously showed that our modified, less invasive LDF procedure can be performed serially without inducing inflammation or gait abnormalities [7]. After 6-8 hours of fasting, anesthesia was induced with 4% isoflurane in pure oxygen and maintained with about 2% isoflurane throughout the 15- to 20-minute-long procedure. The fur over both proximal tibiae was shaved. Mice were placed supine on a heated pad, and the hindlimbs were secured with tape. Using the same methods as described above, an incision was made over one tibia, the periosteum was gently removed, and the LDF needle probe was placed firmly against bone with the micromanipulator. A 30-sec measurement was recorded, the probe was removed and repositioned, and a second 30-sec measurement was recorded. The incision was closed with tissue adhesive, and triple antibiotic ointment and lidocaine cream were applied. The procedure was repeated for the contralateral tibia. Each weekly perfusion measurement was composed of the weighted mean of the two 30-sec long measurements for that bone.

Osteovascular Structure (Femur)

Osteovascular structure was examined in the subset of affected and unaffected femora stored in PBS using contrast-enhanced micro-computed tomography (CE-CT). Each femur was cut in half transversely with a scalpel, and the distal halves were incubated in a 3.695 mmol/L staining solution of hafnium-substituted Wells-Dawson polyoxometalate hydrate ($K_{16}[Hf(\alpha_2$-

$P_2W_{17}O_{61})_2]\bullet 19H_2O$) (Hf-POM) in 1 mL PBS for 48 hours at 4°C, with gentle shaking according to a previously described protocol [8]. Samples were scanned with a phoenix nanotom® m (GE Measurement and Control Solutions, Wunstorf, Germany) using 60 kV peak X-ray tube potential, 140 µA X-ray intensity, and 500-ms integration time. A 0.1-mm-thick aluminum filter was applied to reduce beam hardening. Because of the relatively high X-ray attenuation of the Hf-POM-stained samples, a diamond-coated tungsten target was applied. Volumes were reconstructed at an isotropic voxel size of 2 µm using the GE datos|x software with a beam hardening correction setting of 7 and a Gaussian filter setting of 3.

Blood vessel and adipocyte microstructure was assessed in a manually selected volume of interest (VOI) that was 1.6-mm long (about 10% average femur length), starting from the distal growth plate and extending proximally into the metaphysis, excluding cortical bone tissue, using the CTAn software (Bruker MicroCT, Kontich, Belgium). Within this VOI, cancellous bone was segmented, binarized via automatic 3D Otsu segmentation, and subtracted from the image, leaving the marrow volume. A manual global thresholding method was used to segment blood vessels and adipocytes. First, the adipocytes were binarized using opening (sphere with 1-voxel radius), closing (sphere with 3-voxel radius), and two despeckling (remove white and black speckles less than 650 voxels) operations. Then the adipocyte volume fraction (adipocyte volume/marrow volume, Ad.V/Ma.V, %), adipocyte density (Ad.D, #/mm^3), and distribution of adipocyte thickness (Ad.Th, µm) were quantified. Second, to eliminate edge artifacts due to the partial volume effect, the adipocytes were dilated (sphere with 5-voxel radius) and subtracted from the images, which made the adipocyte edges have similar grayscale values as those of the blood vessels. The images were then segmented to binarize the blood vessels using closing (sphere with 4-voxel radius), despeckling (remove continuous volumes less than 1,050 voxels), closing (sphere

with 6-voxel radius), and despeckling (remove continuous volumes less than 5,500 voxels) steps. The vessel volume fraction (vessel volume/marrow volume, Ves.V/Ma.V, %), vessel density (Ves.D, #/mm^3), and the distribution of vessel thickness (Ves.Th, µm) were calculated.

Branching parameters of the osteovascular network, including total number of branches, number of junctions, number of triple points (e.g., junctions with three branches), and number of quadruple points (e.g., junctions with four branches), were quantified using the 'Skeleton 3D' and 'Analyze Skeleton' plugins in BoneJ (FIJI v. 1.51n) [9,10], applied to the binarized blood vessels. The distance between blood vessels and bone surfaces was calculated with custom code in MATLAB® (R2018, The MathWorks, Natick, MA). The proximity of blood vessels to bone surfaces was also examined. Similar to the procedure described above, a 1.6-mm-long VOI was manually selected in Slicer (v. 4.11.0) [11], starting at the distal growth plate and extending proximally into the diaphysis, including the cortical bone. The VOI was exported to MATLAB®, and bone tissue, adipocytes, and blood vessels were binarized and processed using the same global threshold values and processing steps described above. The distribution of distances between blood vessel surfaces and bone surfaces (Ves.S-BS distance) was calculated using the 'bwgeodesic' function in MATLAB®.

Osteovascular Composition (Tibia)

Osteovascular composition was examined using immunofluorescence confocal microscopy in bone tissue sections from a subset of affected tibiae (n = 3 sham-sedentary, n = 2 sham-exercise, n = 5 stroke-sedentary, n = 4 stroke-exercise) labeled for markers of non-arterial endothelial cells (endomucin, EMCN) and endothelial cells in sinuses, arterioles, venules, and capillaries (CD31) [12,13]. Blood vessels that are positive for both EMCN and CD31 (defined as

Type H) have been shown to regulate bone-vascular crosstalk and couple osteo- and angiogenesis in long bones [14]. Tibiae were cut transversely at the tibiofibular junction under constant water irrigation with a low speed precision saw fitted with a diamond blade (IsoMet Low Speed Precision Cutter, Buehler, Lake Bluff, IL). The proximal halves of the tibiae were decalcified for 24 hours at 4°C with constant agitation in a solution of 0.342 mol/L ethylenediaminetetraacetic acid (Fisher Scientific, Hampton, NH) diluted in 1X PBS at pH 7.6. Bone samples were then prepared for sectioning and staining with immunofluorescence markers [15]. Briefly, decalcified tissue was infiltrated with a cryoprotectant solution (0.584 mol/L sucrose (S7903, Sigma-Aldrich, St. Louis, MO) and 5.556E-5 mol/L polyvinylpyrrolidone (P5288, Sigma-Aldrich) in 1X PBS) at 4°C for 24 hours with constant agitation. Next, samples were incubated in an embedding media (0.267 mol/L gelatin from porcine skin (G1890, Sigma-Aldrich), 0.584 mol/L sucrose, and 5.556E-5 mol/L polyvinylpyrrolidone in 1 X PBS) at 60°C for 45 min, room temperature for 30 min, and then stored at -80°C until sectioned. In each proximal sample, 50-µm-thick longitudinal sections were obtained using a cryostat at -23°C (HN 525NX, Thermo Fisher Scientific, Waltham, MA). Sections were dried at room temperature for 30 min and then stored at -20°C.

For immunofluorescence staining, slides were equilibrated to room temperature for 30 min, then rehydrated in 1X PBS for 5 min. Sections were permeabilized with a solution of 4.638E-3 mol/L Triton X (T8787, Sigma-Aldrich) diluted in 1X PBS for 20 min at room temperature and blocked in a solution of donkey serum diluted 1:20 in 1X PBS for 30 min at room temperature. Sections were stained using unconjugated antibodies at 1:100 for EMCN (rat anti-mouse sc-65495, Santa Cruz Biotechnology, Santa Cruz, CA), CD31 (hamster anti-mouse ab119341, Abcam, Cambridge, UK), and either vascular endothelial growth factor receptor 2 (VEGFR-2, rabbit anti-mouse ab2349, Abcam) or osteocalcin (rabbit anti-mouse, ab93876, Abcam), with 7.728E-5 mol/L

Triton X diluted in 1X PBS at 4°C overnight. Secondary antibodies were added at 1:200 (goat anti-rat with AlexaFluor 647 ab150159, Abcam; goat anti-hamster with AlexaFluor 568 A21112 Invitrogen, Carlsbad, CA; and goat anti-rabbit 488 A11034, Invitrogen) with 7.728E-5 mol/L Triton X diluted in 1X PBS for 60 min at room temperature. Nuclear staining was performed with a 7.212E-6 mol/L solution of DAPI diluted in 1X PBS incubated for 10 min at room temperature.

Sections were imaged immediately following staining at 20X on a Zeiss Laser Scanning Microscope 880 with Airyscan (Carl Zeiss Microscopy, Thornwood, NY), and the areas of, CD31-positive, EMCN-positive, and Type H vessels, relative to total area, were quantified. Tile scan images were stitched and processed into maximum intensity projections using the microscope software (Zen 2.3 SP1, Carl Zeiss Microscopy). Regions of interest (ROIs) equal to 10% of tibia length were drawn in FIJI, starting at the proximal growth plate and extending distally into the metaphysis. CD31-positive regions inside the ROI were manually traced into masks in FIJI. Using custom code in MATLAB®, EMCN-positive regions were automatically binarized with an adaptive threshold, and then the mask was refined with an opening (disk with 1-pixel radius) followed by a closing (disk with 2-pixel radius) operation. The CD31 mask, EMCN mask, and the intersection of both masks (Type H) were calculated in FIJI. Staining for VEGFR-2 and osteocalcin was indistinguishable from background and could not be quantified. Osteovascular composition parameters were measured in two sections per bone, and the mean values were used for analysis.

Statistical Analyses

Statistical models were analyzed with SAS (SAS University Edition v. 9.4, SAS Institute Inc., Cary, NC) with a significance level of 0.05. Statistical models were designed to determine

the following: 1) effect of ischemic stroke and exercise on intraosseous perfusion during stroke recovery; 2) acute effect of ischemic stroke on intraosseous perfusion during surgery; 3) effect of stroke and exercise on osteovascular structure and composition; and 4) whether stroke differentially affects intraosseous perfusion or osteovascular structure in the affected vs. unaffected limb.

For analysis #1, LDF measures of perfusion were compared between surgery and activity groups at each timepoint and limb using a mixed hierarchical linear model (procedure GLIMMIX) with interaction between all terms [16]. Each mouse was considered a subject (replicate), assigned randomly to a group comprised of the combination of surgery and activity groups. Surgery groups (sham or stroke) and activity groups (sedentary or exercise) were modeled as fixed factors, limb as a nested within-subject factor, and timepoint as a longitudinal repeated measure. LDF was measured across four timepoints (Weeks 1-4) at each observational unit (each limb of each mouse). Variation among subjects within each group combination (i.e., sham-sedentary) was considered a random effect. Residuals were modeled using a compound symmetry covariance structure. A modified Kenward-Roger approximation was used to calculate denominator degrees of freedom and standard error of fixed effects [16]. Effect differences between surgery and activity groups were compared within each timepoint (i.e., stroke-exercise vs. stroke-sedentary at Week 2) using least squares means and Tukey-Kramer adjustments for multiple comparisons.

For analysis #2, the stability of the tibial perfusion measurements throughout the surgery was examined using the slope of the 30-minute LDF measurement taken during the surgical procedure. To determine if the slope for each group was different from zero, which would indicate that the perfusion measurement varied and was not stable, an unpaired t-test was performed for the

sham group, and a Wilcoxon rank sum test was performed for the stroke group. Slopes were also compared between the stroke and sham groups with a Wilcoxon two-sample test.

For analysis #3, distribution data from CE-CT (vessel thickness, blood vessel surface to bone surface distance) were compared between surgery and activity groups using a mixed hierarchical linear model (procedure GLIMMIX) with interaction between terms. The model was similar to the model used for analysis #1, except the repeated factor 'week' was replaced with histogram 'bins'. Variation among subjects within each group combination (i.e., sham-sedentary) was considered a random effect that was modeled with a heterogenous variance components method across each surgery group (sham or stroke). Variation among each group combination was modeled as an intercept for each group linear predictor. A modified Kenward-Roger approximation was used to calculate denominator degrees of freedom and standard error of fixed effects. Effect differences were compared between groups within histogram bins (i.e., stroke-exercise vs. stroke-sedentary within bin 'a') using least squares means with Tukey-Kramer adjustments for multiple comparisons. All other CE-CT parameters (Ad.V/Ma.V, average Ad.Th, Ad.D, Ves.V/Ma.V, average Ves.Th, Ves.D, branches, junctions, triple points, and quadruple points) were compared between surgery and activity groups using a repeated measures factorial model (procedure MIXED) with interaction between terms. Surgery and activity groups were modeled as fixed factors, while limb was modeled as a repeated measure. Residual variance was modeled with compound symmetry covariance, and effect differences were compared between groups using least squares means with Tukey-Kramer adjustments for multiple comparisons. Immunofluorescence parameters were compared between surgery and activity groups using a standard two-factor general linear model (procedure GLM) with interaction and Tukey adjustments for multiple comparisons.

For analysis #4, the same repeated measures models from analyses 1 and 3 were used, but least squares means were compared between limbs within surgery group (i.e., affected vs. unaffected side within the stroke group).

Supplemental References

[1] E.Z. Longa, P.R. Weinstein, S. Carlson, R. Cummins, Reversible middle cerebral artery occlusion without craniectomy in rats., Stroke. 20 (1989) 84–91. doi:10.1161/01.STR.20.1.84.

[2] J. Koizumi, Y. Yoshida, T. Nakazawa, G. Ooneda, Experimental studies of ischemic brain edema, I: a new experimental model of cerebral embolism in rats in which recirculation can be introduced in the ischemic area, Jnp J Stroke. 8 (1986).

[3] H. Sakai, H. Sheng, R.B. Yates, K. Ishida, R.D. Pearlstein, D.S. Warner, Isoflurane provides long-term protection against focal cerebral ischemia in the rat, Anesthesiology. 106 (2007) 92–99; discussion 8-10.

[4] N.J. Hanne, A.J. Steward, M.R. Sessions, H.L. Thornburg, H. Sheng, J.H. Cole, Stroke prevents exercise-induced gains in bone microstructure but not composition in mice, BioRxiv. (2019) 708388. doi:10.1101/708388.

[5] N.J. Hanne, E.D. Easter, S. Stangeland-Molo, J.H. Cole, A Minimally Invasive Technique for Serial Intraosseous Perfusion Measurements in the Murine Tibia Using Laser Doppler Flowmetry, BioRxiv. (2019) 708453. doi:10.1101/708453.

[6] J.F. Griffith, D.K. Yeung, P.H. Tsang, K.C. Choi, T.C. Kwok, A.T. Ahuja, K.S. Leung, P.C. Leung, Compromised Bone Marrow Perfusion in Osteoporosis, J Bone Miner Res. 23 (2008) 1068–1075. doi:10.1359/jbmr.080233.

[7] N.J. Hanne, E.D. Easter, J.H. Cole, Validating Minimally Invasive Laser Doppler Flowmetry for Serial Bone Perfusion Measurements in Mice, BioRxiv. (2019) 708412. doi:10.1101/708412.

[8] G. Kerckhofs, S. Stegen, N. van Gastel, A. Sap, G. Falgayrac, G. Penel, M. Durand, F.P. Luyten, L. Geris, K. Vandamme, T. Parac-Vogt, G. Carmeliet, Simultaneous three-dimensional visualization of mineralized and soft skeletal tissues by a novel microCT contrast agent with polyoxometalate structure, BIomater. 159 (2018) 1–12. doi:10.1016/j.biomaterials.2017.12.016.

[9] M. Doube, M.M. Kłosowski, I. Arganda-Carreras, F.P. Cordelières, R.P. Dougherty, J.S. Jackson, B. Schmid, J.R. Hutchinson, S.J. Shefelbine, BoneJ: Free and extensible bone image analysis in ImageJ, Bone. 47 (2010) 1076–1079. doi:10.1016/j.bone.2010.08.023.

[10] J. Schindelin, I. Arganda-Carreras, E. Frise, V. Kaynig, M. Longair, T. Pietzsch, S. Preibisch, C. Rueden, S. Saalfeld, B. Schmid, J.-Y. Tinevez, D.J. White, V. Hartenstein, K. Eliceiri, P. Tomancak, A. Cardona, Fiji: an open-source platform for biological-image analysis, Nature Methods. 9 (2012) 676–682. doi:10.1038/nmeth.2019.

[11] A. Fedorov, R. Beichel, J. Kalpathy-Cramer, J. Finet, J.-C. Fillion-Robin, S. Pujol, C. Bauer, D. Jennings, F. Fennessy, M. Sonka, J. Buatti, S. Aylward, J.V. Miller, S. Pieper, R. Kikinis, 3D Slicer as an Image Computing Platform for the Quantitative Imaging Network, Magn Reson Imaging. 30 (2012) 1323–1341. doi:10.1016/j.mri.2012.05.001.

[12] S.K. Ramasamy, A.P. Kusumbe, L. Wang, R.H. Adams, Endothelial Notch activity promotes angiogenesis and osteogenesis in bone, Nature. 507 (2014) 376–380. doi:10.1038/nature13146.

[13] M.P. Pusztaszeri, W. Seelentag, F.T. Bosman, Immunohistochemical expression of endothelial markers CD31, CD34, von Willebrand factor, and Fli-1 in normal human tissues, J. Histochem. Cytochem. 54 (2006) 385–395. doi:10.1369/jhc.4A6514.2005.

[14] A.P. Kusumbe, S.K. Ramasamy, R.H. Adams, Coupling of angiogenesis and osteogenesis by a specific vessel subtype in bone, Nature. 507 (2014) 323–328. doi:10.1038/nature13145.

[15] A.P. Kusumbe, S.K. Ramasamy, A. Starsichova, R.H. Adams, Sample preparation for high-resolution 3D confocal imaging of mouse skeletal tissue, Nat. Protoc. 10 (2015) 1904–1914. doi:http://dx.doi.org.prox.lib.ncsu.edu/10.1038/nprot.2015.125.

[16] R.C. Littell, ed., SAS for mixed models, 2nd ed, SAS Institute, Inc, Cary, N.C, 2006.